Hybrid polaritons in a resonant inorganic/organic semiconductor microcavity

M. Höfner,[1,a)] S. Sadofev,[1] B. Kobin,[2] S. Hecht,[2] and F. Henneberger[1,b)]
[1]*Institut für Physik, Humboldt-Universität zu Berlin, Newtonstr.15, 12489 Berlin, Germany*
[2]*Institut für Chemie, Humboldt-Universität zu Berlin, Brook-Taylor-Str. 2, 12489 Berlin, Germany*

(Received 16 July 2015; accepted 18 October 2015; published online 3 November 2015)

We demonstrated the strong coupling regime in a hybrid inorganic-organic microcavity consisting of (Zn,Mg)O quantum wells and ladder-type oligo(*p*-phenylene) molecules embedded in a polymer matrix. A Fabry-Pérot cavity is formed by an epitaxially grown lower ZnMgO Bragg reflector and a dielectric mirror deposited atop of the organic layer. A clear anticrossing behavior of the polariton branches related to the Wannier-Mott and Frenkel excitons, and the cavity photon mode with a Rabi-splitting reaching 50 meV, is clearly identified by angular-dependent reflectivity measurements at low temperature. By tailoring the structural design, an equal mixing with weights of about 0.3 for all three resonances is achieved for the middle polariton branch at an incidence angle of about 35°. © *2015 AIP Publishing LLC*. [http://dx.doi.org/10.1063/1.4934844]

Exciton polaritons in semiconductor microcavities (MCs) have attracted continuous interest over the recent years as these coupled light-matter quasi-particles offer many fascinating features such as parametric amplification,[1,2] Bose-Einstein condensation,[3] and laser action.[4] The first demonstration of strong exciton-photon coupling in an MC is succeeded by employing the enhanced oscillator strength of the Wannier-Mott exciton in an inorganic GaAs/GaAlAs multiple quantum well (MQW) structure.[5] While initially limited to cryogenic temperatures, persistence of polaritons up to room temperature was more recently demonstrated by embedding wide-band-gap semiconductors (GaN[6] and ZnO[7,8]). The fact that conjugated organic molecules exhibit very strong optical transition dipoles has triggered work on these materials as well,[9–12] also reporting on lasing[13] and Bose-Einstein condensation[14] of polaritons related to Frenkel excitons. Here, the Rabi-splitting characterizing the exciton-photon coupling strength is typically one order of magnitude larger than for inorganic Wannier-Mott excitons in the MCs assuring formation of the robust polaritonic entities. However, disorder characteristic of molecular materials and relaxation bottlenecks related to the absence of efficient inelastic scattering processes represent severe obstacles towards practical use. In a proposal made way back in 1997,[15] a hybrid cavity combining inorganic and organic semiconductors was theoretically analysed. It was shown that the merger of the strong optical coupling provided by the Frenkel exciton with the efficient relaxation pathways of the extended Wannier-Mott exciton should result in an unprecedented figure-of-merit for light emission, unattainable by the MCs of the sole materials. Some degree of mixing of Frenkel, Wannier-Mott excitons, and cavity photons could be demonstrated on various types of hybrid MCs.[16–18,25] We demonstrate a system where equal mixing ratio between all three components is reached by adjusting the detuning of the organic monomer and the oscillator strength of both active materials.

In what follows, both, distributed-Bragg-reflectors (DBR) as well as MQW structures, realized by the inorganic ternary (Zn,Mg)O (Ref. 20), are used to create a cavity mirror and the active region with strong Wannier-Mott exciton features at the same time. On the organic side, we employ ladder-type *p*-quaterphenyl (L4P). Because of its rigid planar geometry, this molecule exhibits mirror-symmetric, weakly Stokes-shifted absorption, and emission spectra featuring well-resolved vibronic progressions.[21] Laser action and strong-coupling of a spiro derivative of L4P in a purely organic MC was observed earlier.[22] In contrast to the spiro derivative, the pure L4P is used in the present MC because of the better energetic matching of its (0,0) transition with the excitonic resonance of the ZnO QWs.

The (Zn,Mg)O-based inorganic part of the structure [Fig. 1(a)] consisting of a lower DBR and an MQW region was monolithically grown by molecular beam epitaxy on an a-plane sapphire substrate as described earlier.[19] Overall, 14 alternating $Zn_{0.88}Mg_{0.12}O/Zn_{0.65}Mg_{0.35}O$ layer pairs were deposited to ensure a maximum DBR reflectivity of about 70% in proximity of the ZnO QW exciton absorption. Six 3.5-nm thick $ZnO/Zn_{0.88}Mg_{0.12}O$ QWs were grown atop the ZnMgO DBR and positioned in the vicinity of the antinodes of the electric field. The relatively low reflectivity value of the ZnMgO-based mirror is selected to provide an optical access to the resonance features and still enable the strong coupling regime. The organic layer was deposited by spin-coating the sample with a solution of 17 g/l Zeonex 480 (a cyclo olefin polymer provided by the Zeon Corporation) in toluene containing 27 wt. % of L4P molecules. Because of its high glass transition temperature (140 °C), the polymer sustains the evaporation of a dielectric mirror on top. The concentration of L4P in the polymer was chosen to compensate for the difference in oscillator strength between the molecules and ZnO QWs. The total thickness of the organic layer was about 120 nm. The top dielectric mirror formed by 5 layer pairs of SiO_x and ZrO_x was then deposited by electron beam evaporation. During the evaporation, the sample was heated up to $T_s \approx 100$ °C, providing a reasonable

a)Electronic mail: mhoefner@physik.hu-berlin.de
b)Deceased.

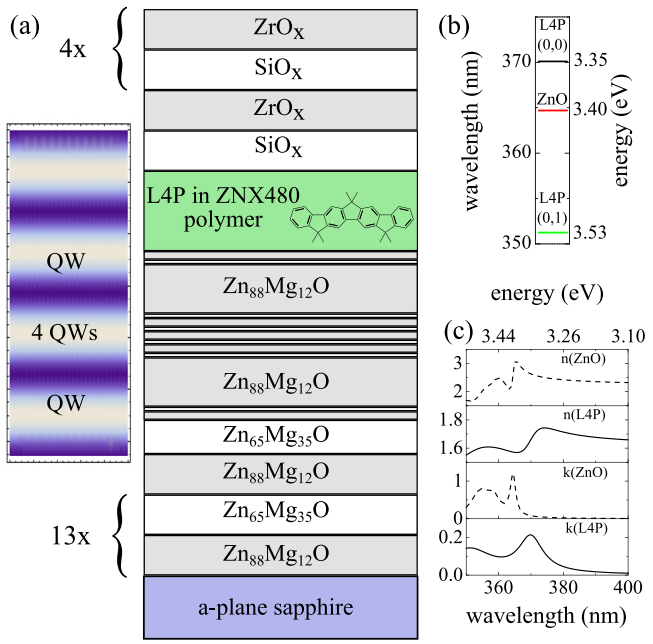

FIG. 1. (a) Schematic layout of a sample (proportional to their optical thickness) consisting of a lower DBR with 14 pairs of $Zn_{88}Mg_{12}O/Zn_{65}Mg_{35}O$ layers, 6 $ZnO/Zn_{88}Mg_{12}O$ QWs positioned in the antinodes of the electric field, an organic layer containing L4P in a polymer matrix (27 wt. %), and a top DBR composed of 5 pairs of SiO_x and ZrO_x layers. The schematic field distribution inside the cavity is shown on the left by the color plot to visualize the positioning of the QWs. (b) Energetic position of the uncoupled absorption resonances at $T = 5$ K. The relevant resonances are the (0,0) vibronic transition of L4P and the ZnO QW absorption. (c) Imaginary and real parts of the complex refractive index of the molecule/polymer layer (full line) and a typical ZnO QW (dashed lines) at low temperature.

compromise between the sample temperature needed to achieve high optical quality of the mirror and the mechanical stability of the polymer layer.[23] The design of the cavity is shown in Figure 1(a), and the energetic positions of the absorption resonances of ZnO QWs and L4P are schematically shown in Figure 1(b). The complex refractive index with its real part n and imaginary part k for both active materials is shown in Figure 1(c). The extinction coefficient k presented for the organic layer is for the mix of polymer and L4P, not for the pure molecule. The measurements were performed for a single spin coated layer of a reference sample. The absorption data were fitted by a Lorentz oscillator model for the dielectric function to create the complex refractive index presented and used to design the cavity structure. Two oscillators of the form $f/(\hbar^2(\omega_0^2 - \omega^2 - i\gamma\omega))$ and a background dielectric constant of $\epsilon_B = 2.56$ were used to model the organic layer, and three oscillators and $\epsilon_B = 4.84$ for the ZnO QWs, respectively.

The angular resolved reflection measurements were performed from the front side of the sample in a transmission cryostat connected to a home-built goniometer table at 5 K. A tungsten lamp was used as a light source. The incident light was linear polarized to avoid a transverse electric/-magnetic polarization-splitting of the cavity mode, and the reflected light was detected through an optical fiber with a 1 mm core diameter without any light collecting optics. The fiber was adjusted with a precision of $\pm 0.5°$ and was imaged on a slit of a spectrometer with a charge coupled device for detection.

Figure 2 displays the normal incidence transmission spectra of the epitaxially grown sample part and the dielectric mirror deposited on top as measured on a reference sample. The transmission spectrum of the bare inorganic part of the structure (black curve) reveals a photonic stop-band with a bandwidth of about 140 meV centered at $E_{\text{lower DBR}} = 3.31$ eV. The absorption of the ZnO QWs appears as a dip at the edge of the stopband at $E_{ZnO} = 3.39$ eV. At even shorter wavelengths, the transmission rapidly decreases due to the absorption of the high refractive index layer of the DBR. The stop-band of the top dielectric mirror (red curve) centered at $E_{\text{upper DBR}} \approx 3.10$ eV is much broader compared to that of the lower DBR, and reaches a maximum reflectivity of about 90%. The reflection spectrum of the entire structure (green curve), measured at an angle of incidence of 10°, clearly shows the formation of the cavity mode at $E_{cav} = 3.26$ eV, that is, about 90 meV red shifted compared to the (0,0) absorption resonance of the L4P [Fig. 1(b)].

The dispersion curves for the excitonic and photonic resonances were probed by angular-dependent reflectivity measurements. The change in the angle of incidence corresponds to a tuning of the cavity resonance as shown in the following equation:

$$\omega_c(\theta) = \frac{\omega(0)}{\sqrt{1 - \frac{\sin^2(\theta)}{n_{\text{eff}}^2}}}, \tag{1}$$

where θ is the angle of incidence, $\omega(0)$ is the undisturbed cavity frequency at $\theta = 0°$, and n_{eff} is the effective refractive index of the whole structure, determining the tuning range.

Figure 3 depicts the reflection spectra of the structure at different angles of incidence θ shown for clarity in steps of 5° (measured in steps of 1°). At $\theta = 15°$, the spectrum is dominated by the cavity mode centered at $E_{cav} = 3.29$ eV. A weak absorption feature related to the Frenkel exciton in the organic layer is also visible at $E_{L4P} = 3.37$ eV, i.e., already slightly shifted due to coupling. At $\theta = 40°$, all three

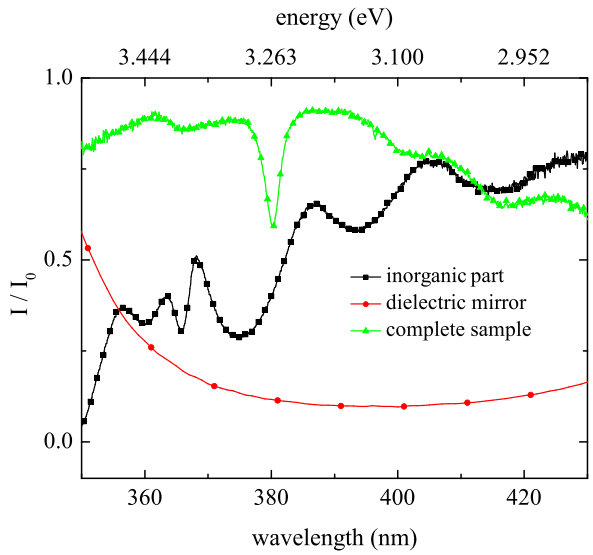

FIG. 2. Transmission of the inorganic cavity part (black squares, $T = 77$ K), the dielectric top mirror on a reference sample (red circles, $T = 300$ K), and reflection spectrum of the whole structure (green triangles, $T = 5$ K).

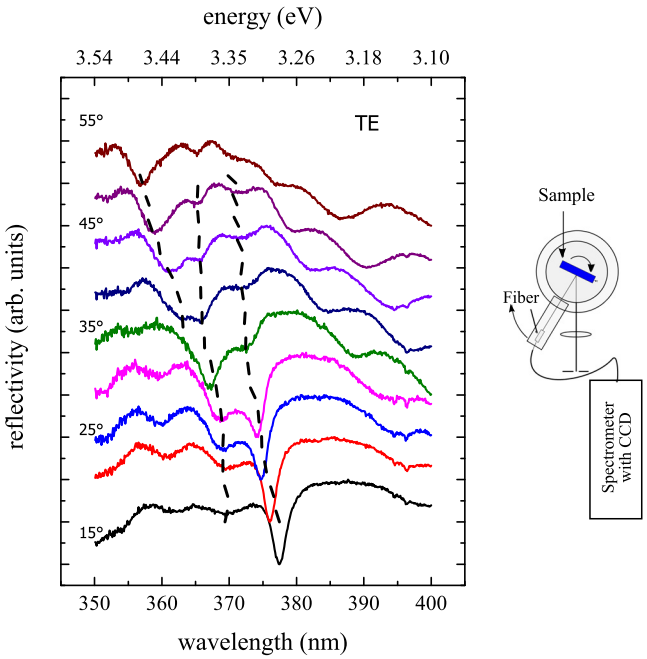

FIG. 3. Left: Angular-resolved reflectivity spectra measured with TE polarized light at 5 K (horizontally shifted for clarity). Dashed lines give the reflection minima corresponding to the polariton resonances for the whole set of spectra. Right: Measuring geometry used.

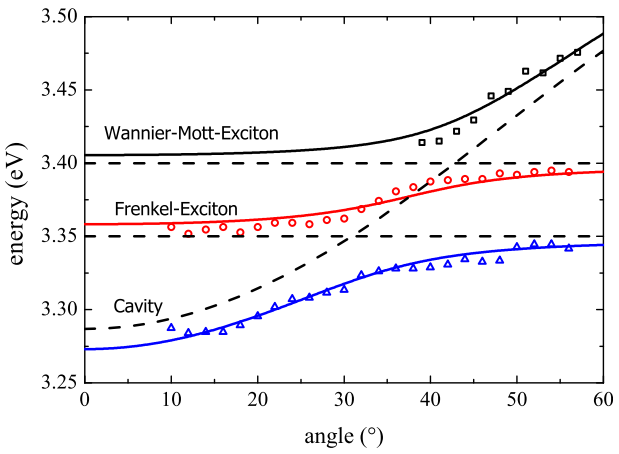

FIG. 4. Angular dependence of the energetic position of the reflection minima. Symbols: experimental reflection minima, lines: fits by the oscillator model with $V_{\mathrm{L4P}} = 27\,\mathrm{meV}$, $V_{\mathrm{ZnO}} = 24\,\mathrm{meV}$, $\mathrm{n_{eff}} = 2.66$, and $\hbar\omega_c(0) = 3.29\,\mathrm{eV}$. The undisturbed excitonic resonances and the cavity dispersion are shown by the dashed lines.

resonances related to the lower, middle, and upper polariton branches become clearly visible. The black dashed lines represent the energy positions of the reflection minima of the measured spectra demonstrating typical anticrossing behavior expected for the strong coupling regime.

The positions of the minima extracted from the reflection data were fitted by a coupled oscillator model for three resonances [Eq. (2)] with the coupling constants $(V_{\mathrm{L4P}}, V_{\mathrm{ZnO}})$, the effective refractive index ($\mathrm{n_{eff}}$), and the cavity resonance at zero incidence angle ($\hbar\omega(0)$) as the fitting parameters[16,24,25]

$$\begin{pmatrix} E_{\mathrm{ZnO}} & 0 & V_{\mathrm{ZnO}} \\ 0 & E_{\mathrm{L4P}} & V_{\mathrm{L4P}} \\ V_{\mathrm{ZnO}} & V_{\mathrm{L4P}} & \hbar\omega_c(\theta) \end{pmatrix} \begin{pmatrix} v_1 \\ v_2 \\ v_3 \end{pmatrix}_i (\theta) = E_i(\theta) \begin{pmatrix} v_1 \\ v_2 \\ v_3 \end{pmatrix}_i (\theta). \tag{2}$$

The result is summarized in Figure 4. The dashed lines mark the positions of the uncoupled excitonic resonances and the dispersion of the uncoupled cavity mode given by Eq. (1) with $\hbar\omega(0) = 3.29\,\mathrm{meV}$ and $\mathrm{n_{eff}} = 2.66$. The three-angle dependent eigenvalues $\mathrm{E}_i(\theta)$ of the matrix are energetically shifted compared to the unperturbed resonances due to the coupling. Good agreement to experimental data is found for the coupling constants $V_{\mathrm{ZnO}} \approx V_{\mathrm{L4P}} \approx 25\,\mathrm{meV} \pm 5\,\mathrm{meV}$. This is slightly stronger than the coupling of the QWs in the monolithic MC presented in Ref. 20 and about half of the pure organic cavity based on the spiro derivative of L4P,[22] reduced by the higher cavity length.

The contributions (weights) given by the square of eigenvectors of the coupling matrix ($|v_1|^2$, $|v_2|^2$, $|v_3|^2$) are shown in Figure 5. While the lower and upper branches demonstrate mixing of the photon mode with only a single type of exciton, equal mixing coefficients are reached for all three oscillators in the middle branch. Here, the polariton state has mostly Frenkel excitonic character at small angles. By increasing the angle of incidence, thereby increasing the in-plane wave-vector, the contribution of the Frenkel exciton gradually decreases and the excitation is equally distributed between all involved resonances. At very high angles, the character of the polariton state is dominated by the Wannier-Mott exciton. Thus, a truly hybrid exciton polariton with a mixed photon-, Frenkel- and Wannier-Mott character is created at the angle of incidence of 35°. The values for the coupling constants and effective refractive index change only slightly in TM polarization, which is therefore not shown

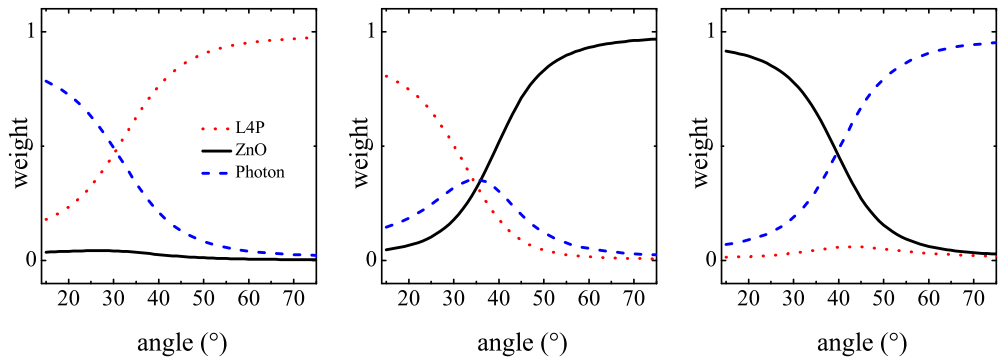

FIG. 5. Mixing fraction for the lower (left), middle (center), and upper (right) branch.

here. The mixed character of the exciton polariton in the middle branch and the energy splitting of 50 meV, which is close to the energy of longitudinal optical phonons in ZnO (72 meV), create the prerequisites for a very efficient phonon assisted relaxation. Such processes can help to overcome the emission bottleneck, which has recently been demonstrated in bulk ZnO polariton lasers.[26]

In conclusion, we created a hybrid cavity based on inorganic ZnO QWs and a specially synthesized organic molecule (L4P) in resonance to the QW absorption, which makes the coupling of both excitonic resonances at the same k-vector possible. The angular resolved reflectivity measurements give clear evidence for strong coupling of the resonances, with equal mixing of the three resonances. The treatment of the experimental data within the three coupled oscillator model provides the coupling constants of ≈25 meV. An increase in the coupling strength to 36 meV by raising the density of oscillators in the cavity to match the phonon energy should make both an efficient polariton relaxation and room temperature polariton formation possible. Furthermore, the photonic weights are tailored by adjusting the oscillator strength of the active materials, creating a hybrid state with equally distributed weights among all three resonances. Since both materials are vacuum processable, cavities with higher quality factors are just a question of fabrication technique, making ZnO and L4P excellent candidates for tailoring the phonon assisted polariton relaxation to create a hybrid polariton laser operating at room temperature.

The authors like to thank E. Renger for her support in sample fabrication, H.-J. Wünsche, S. Blumstengel, and O. Benson for the fruitful discussion and support.

This work was supported by the Deutsche Forschungsgemeinschaft in the frame of CRC 951 (HIOS). M. H. also acknowledges the financial support from IRTG 1740, the Sao Paulo Research Foundation (FAPESP) in TRP 2011/50151-0, and the Helmholtz Alliance for Photovoltaics.

[1]P. V. Kelkar, V. G. Kozlov, A. V. Nurmikko, C.-C. Chu, J. Han, and R. L. Gunshor, Phys. Rev. B **56**, 7564 (1997).
[2]M. Saba, C. Ciuti, J. Bloch, V. Thierry-Mieg, R. André, L. Si Dang, S. Kundermann, A. Mura, G. Bongiovanni, J. L. Staehli, and B. Deveaud, Nature (London) **414**, 731 (2001).
[3]J. Kasprzak, M. Richard, S. Kundermann, A. Baas, P. Jeambrun, J. M. J. Keeling, F. M. Marchetti, M. H. Szymańska, R. André, J. L. Staehli, V. Savona, P. B. Littlewood, B. Deveaud, and Le. Si Dang, Nature (London) **443**, 409 (2006).
[4]D. Snoke and P. Littlewood, Phys. Today **63**(8), 42 (2010).
[5]C. Weisbuch, M. Nishioka, A. Ishikawa, and Y. Arakawa, Phys. Rev. Lett. **69**, 3314 (1992).
[6]S. Christopoulos, G. Baldassarri Höger von Högersthal, A. J. D. Grundy, P. G. Lagoudakis, A. V. Kavokin, J. J. Baumberg, G. Christmann, R. Butté, E. Feltin, J.-F. Carlin, and N. Grandjean, Phys. Rev. Lett. **98**, 126405 (2007).
[7]R. Schmidt-Grund, B. Rheinländer, C. Czekalla, G. Benndorf, H. Hochmuth, M. Lorenz, and M. Grundmann, Appl. Phys. B **93**, 331 (2008).
[8]F. Li, L. Orosz, O. Kamoun, S. Bouchoule, C. Brimont, P. Disseix, T. Guillet, X. Lafosse, M. Leroux, J. Leymarie, M. Mexis, M. Mihailovic, G. Patriarche, F. Réveret, D. Solnyshkov, J. Zuniga-Perez, and G. Malpuech, Phys. Rev. Lett. **110**, 196406 (2013).
[9]D. G. Lidzey, D. D. C. Bradley, M. S. Skolnick, T. Virgili, S. Walker, and D. M. Whittaker, Nature (London) **395**, 53 (1998); D. G. Lidzey, D. D. C. Bradley, T. Virgili, A. Armitage, and M. S. Skolnick, Phys. Rev. Lett. **82**, 3316 (1999).
[10]F. Sasaki, S. Haraichi, and S. Kobayashi, Quantum Electron. **38**, 943 (2002).
[11]J. R. Tischler, M. S. Bradley, V. Bulović, J. H. Song, and A. Nurmikko, Phys. Rev. Lett. **95**, 036401 (2005).
[12]T. Schwartz, J. A. Hutchinson, C. Genet, and T. W. Ebbesen, Phys. Rev. Lett. **106**, 196405 (2011).
[13]S. R. J. Holmes and S. R. Forrest, Phys. Rev. Lett. **93**, 186404 (2004).
[14]J. D. Plumhof, T. Stöferle, L. Mai, U. Scherf, and R. F. Mahrt, Nat. Mater. **13**, 247 (2014).
[15]V. Agranovich, H. Benisty, and C. Weisbuch, Solid State Commun. **102**, 631 (1997).
[16]R. J. Holmes, S. Kéna-Cohen, V. M. Menon, and S. R. Forrest, Phys. Rev. B **74**, 235211 (2006).
[17]G. Lanty, S. Zhang, J. S. Lauret, E. Deleporte, P. Audebert, S. Bouchoule, X. Lafosse, J. Zuñiga-Pérez, F. Semond, D. Lagarde, F. Médard, and J. Leymarie, Phys. Rev. B **84**, 195449 (2011).
[18]M. Slootsky, X. Liu, V. M. Menon, and S. R. Forrest, Phys. Rev. Lett. **112**, 076401 (2014).
[19]S. Kalusniak, S. Sadofev, S. Halm, and F. Henneberger, Appl. Phys. Lett. **98**, 011101 (2011).
[20]S. Halm, S. Kalusniak, S. Sadofev, H.-J. Wünsche, and F. Henneberger, Appl. Phys. Lett. **99**, 181121 (2011).
[21]B. Kobin, L. Grubert, S. Blumstengel, F. Henneberger, and S. Hecht, J. Mater. Chem. **22**, 4383 (2012).
[22]M. Höfner, B. Kobin, S. Hecht, and F. Henneberger, Chem. Phys. Chem. **15**, 3805 (2014).
[23]L. Persano, P. Del Carro, E. Mele, R. Cingolani, D. Pisignano, M. Zavelani-Rossi, S. Longhi, and G. Lanzani, Appl. Phys. Lett. **88**, 121110 (2006).
[24]J. Wainstain, C. Delalande, D. Gendt, M. Voos, J. Bloch, V. Thierry-Mieg, and R. Planel, Phys. Rev. B **58**, 7269 (1998).
[25]J. Wenus, R. Parashkov, S. Ceccarelli, A. Brehier, J.-S. Lauret, M. S. Skolnick, E. Deleporte, and D. G. Lidzey, Phys. Rev. B **74**, 235212 (2006).
[26]L. Orosz, F. Réveret, F. Médard, P. Disseix, J. Leymarie, M. Mihailovic, D. Solnyshkov, G. Malpuech, J. Zuniga-Pérez, F. Semond, M. Leroux, S. Bouchoule, X. Lafosse, M. Mexis, C. Brimont, and T. Guillet, Phys. Rev. B **85**, 121201 (2012).